NANO LETTERS

pubs.acs.org/NanoLett Letter

Automated Assembly of Wafer-Scale 2D TMD Heterostructures of Arbitrary Layer Orientation and Stacking Sequence Using Water Dissoluble Salt Substrates

Sang Sub Han, Tae-Jun Ko, Changhyeon Yoo, Mashiyat Sumaiya Shawkat, Hao Li, Bo Kyung Kim, Woong-Ki Hong, Tae-Sung Bae, Hee-Suk Chung, Kyu Hwan Oh, and Yeonwoong Jung*

Cite This: *Nano Lett.* 2020, 20, 3925−3934 Read Online

ACCESS | Metrics & More | Article Recommendations | Supporting Information

ABSTRACT: We report a novel strategy to assemble wafer-scale two-dimensional (2D) transition metal dichalcogenide (TMD) layers of well-defined components and orientations. We directly grew a variety of 2D TMD layers on "water-dissoluble" single-crystalline salt wafers and precisely delaminated them inside water in a chemically benign manner. This manufacturing strategy enables the automated integration of vertically aligned 2D TMD layers as well as 2D/2D heterolayers of arbitrary stacking orders on exotic substrates insensitive to their kind and shape. Furthermore, the original salt wafers can be recycled for additional growths, confirming high process sustainability and scalability. The generality and versatility of this approach have been demonstrated by developing proof-of-concept "all 2D" devices for diverse yet unconventional applications. This study is believed to shed a light on leveraging opportunities of 2D TMD layers toward achieving large-area mechanically reconfigurable devices of various form factors at the industrially demanded scale.

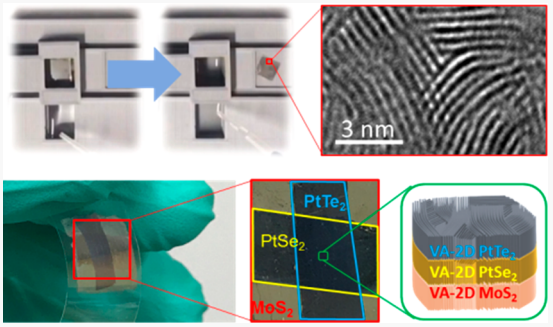

KEYWORDS: *2D layer, 2D TMD, 2D heterolayer, vertically aligned layer, assembly, automation*

INTRODUCTION

Advancements of modern electronics have been driven toward incorporating a large set of previously impossible functionalities such as high mechanical deformability and process sustainability.[1−3] Traditional manufacturing strategies based on bulky three-dimensional silicon (Si) wafers are intrinsically limited in realizing such novel aspects owing to their rigid, complicated, and unsustainable process nature. In this regard, two-dimensional (2D) transition metal dichalcogenide (TMD) layers offer distinct advantages due to their extremely large mechanical tolerance and small thickness as well as van der Waals (vdW) attraction-enabled relaxed assembly requirement.[4−6] Such unparalleled opportunities have triggered proliferating extensive research endeavors as well as piloting industry-oriented initiatives toward emergent technologies.[7−18] While major efforts in fundamental sciences have focused on unveiling their intrinsic properties,[19−22] rapidly growing intellectual property landscapes have already started to leverage them toward practical device applications in a wide range of domains.[7,8,23,24] To this end, it is important to manufacture 2D TMD layers of controlled chemistry and morphology in a way to be compatible with the currently available wafer process schemes. Ultimately, there is demand to develop an "automation" process that will enable the deterministic integration of wafer-scale 2D TMD layers onto target substrates in a controlled and sustainable manner. This approach not only relieves the laborious and delicate handling of individual 2D layers, but this approach also should preserve their intrinsic material properties, minimizing the involvement of quality-impairing chemicals during the integration stages.[8,25−27] Such perspective is particularly essential for realizing 2D TMD heterolayers which require the individual 2D layers of chemically distinct components to be integrated in a layer-by-layer manner.[7,18,23,28−32] Moreover, the integration process should be generic to integrating 2D TMDs irrespective of their crystallographic layer orientation, that is, horizontally or vertically aligned onto substrates of virtually unrestricted forms.

Herein, we developed a versatile and sustainable approach to manufacture wafer-scale 2D TMD layers of arbitrary chemical composition and crystallographic orientation on exotic substrates. This manufacturing scheme adopts the scalable chemical vapor deposition (CVD) growth of 2D TMD layers

Received: March 11, 2020
Revised: April 6, 2020
Published: April 20, 2020

https://dx.doi.org/10.1021/acs.nanolett.0c01089
Nano Lett. 2020, 20, 3925−3934

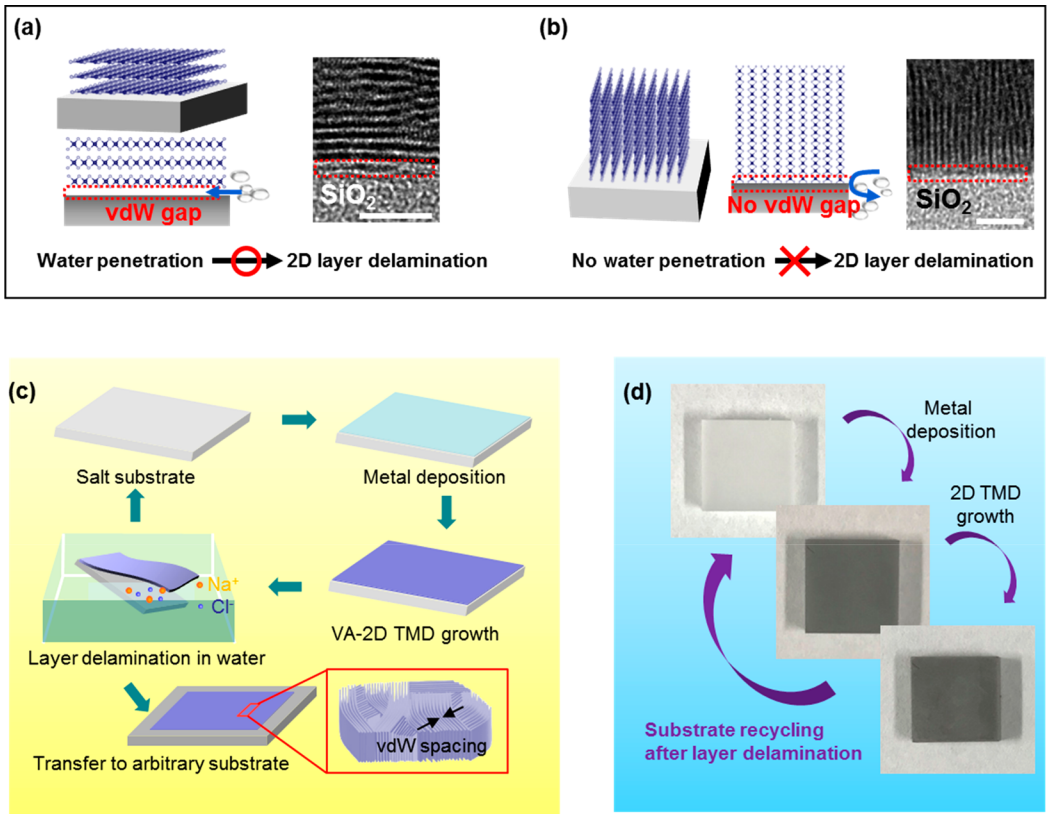

Figure 1. (a,b) Schematic illustrations highlighting the feasibility of water-assisted delamination for (a) HA- and (b) VA-2D TMD layers, and their representative cross-sectional HRTEM images of 2D MoS_2 layers. The scale bars are 5 and 2.5 nm for (a,b), respectively. (c) Schematic illustration of stepwise processes for the water-assisted delamination and transfer of VA-2D TMD layers using salt crystals. (d) Representative images to highlight the sustainability of salt crystals throughout sequential steps of metal deposition, 2D TMD layers growth, and their delamination.

on "water-dissoluble" salt wafers and their spontaneous delamination. We demonstrated the controlled integration of "vertically-aligned" 2D heterolayers of whichever desired layer-stacking orders in a fully automated manner and projected their opportunities for unconventional device applications.

RESULTS AND DISCUSSION

The manufacturing process relies on the water-assisted delamination of CVD-grown wafer-scale 2D TMD layers. Figure 1a,b describes the working principle for 2D TMD layers of distinct layer orientation, that is, horizontally aligned (HA) versus vertically aligned (VA), respectively. It is known that HA-2D TMD layers can be spontaneously delaminated from their growth wafers (e.g., silicon dioxide/silicon (SiO_2/Si)) inside water[33−39] and attributed to the exposure of vdW gaps in between them and the wafers. Figure 1a illustrates this scenario along with a representative cross-sectional high-resolution transmission electron microscopy (HRTEM) image of HA-2D molybdenum disulfide (MoS_2) layers. However, delaminating VA-2D TMD layers has been technically challenging with this approach, as described in Figure 1b. In this case, individual 2D layers are vertically "rooted" in the wafer surface without exposing vdW gaps, impeding their delamination in water as previously verified.[33] This challenge has been the major limiting factor in terms of fully exploring technological opportunities of VA 2D-TMD layers beyond their growth substrate-bound forms. In general, VA 2D-TMD layers exhibit unparalleled chemical reactivity and physisorption properties owing to their surface-exposed rich dangling bonds, suggesting great implications for high-performance electrochemical and/or molecular sensing applications.[40,41] Such unprecedented opportunities can be realized even in flexible and/or stretchable forms as far as they are deterministically and stably integrated on mechanically reconfigurable yet functional substrates retaining their original structural integrity. Figure 1c illustrates schematics of our manufacturing strategy, which overcomes this limitation and can be generalized to 2D TMD layers of any layer orientation. Metal thin films are deposited on single-crystalline salt substrates, and the prepared samples undergo CVD processes adopting the previously developed recipes.[33,35,42−45] The 2D layer orientation can be controlled by adjusting the thickness of the metal films,[45,46] and we focus on growing and delaminating VA-2D layers. As-prepared samples are immersed in water, which causes the spontaneous delamination of only VA-2D layers only within a few seconds after the immersion. The original salt substrates remain nearly intact and can be reused for subsequent CVD growth. The delaminated VA-2D TMD layers floating on the water surface are manually integrated on secondary substrates of desired functionalities, and this entire process can be repeated until targeted 2D TMD heterolayers are achieved. In order to verify the generality and versatility of this approach, we grew a variety of 2D TMD layers including platinum diselenide ($PtSe_2$) and platinum ditelluride ($PtTe_2$) beyond MoS_2 on a variety of salt crystals including sodium chloride (NaCl), potassium chloride (KCl), and potassium bromide (KBr). These substrates have been judiciously selected due to their combined advantage of high melting temperature (up to ~800 °C) and high water solubility.[47] Details for CVD growth conditions are described in Methods. Figure 1d shows

https://dx.doi.org/10.1021/acs.nanolett.0c01089
Nano Lett. 2020, 20, 3925−3934

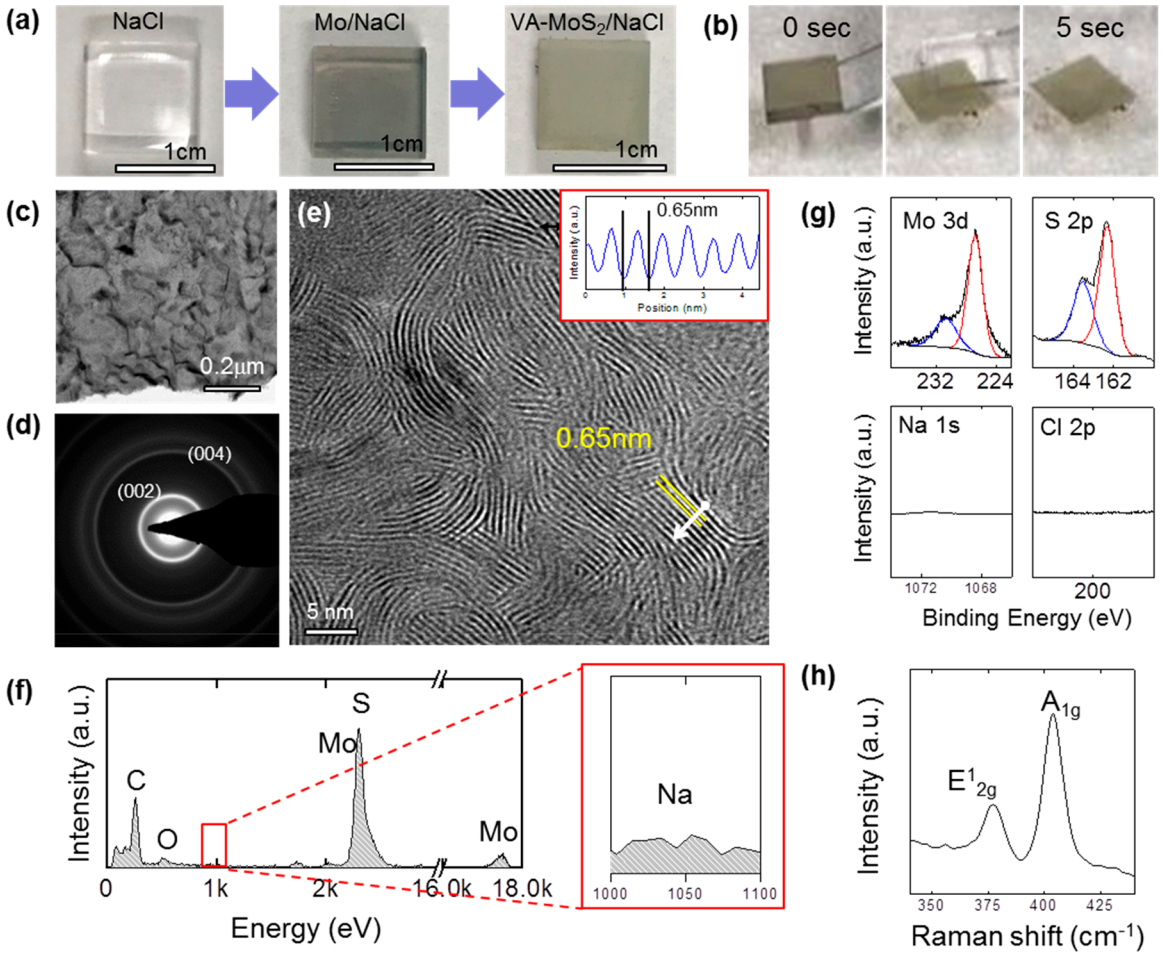

Figure 2. (a) Demonstration of VA-2D MoS_2 layer growth on a single-crystalline NaCl substrate. (b) Time-lapsed snapshot images of delaminating VA-2D MoS_2 layers in water. (c) Low-magnification TEM image, and (d) SAED pattern of delaminated VA-2D MoS_2 layers. (e) HRTEM image of delaminated VA-2D MoS_2 layers denoting the interlayer vdW spacing of 0.65 nm. The inset shows the line intensity profile taken along the white arrow in the TEM image. (f) EDS profile obtained from delaminated VA-2D MoS_2 layers and the enlarged view of the energy range corresponding to Na. (g) XPS profiles of Mo 3d, S 2p, Na 1s, and Cl 2p core levels obtained from delaminated VA-2D MoS_2 layers. (h) Raman spectrum obtained from delaminated VA-2D MoS_2 layers.

photographs corresponding to the step-by-step procedures illustrated in Figure 1c. It is worth mentioning that the salt substrates well retain their surface uniformity and smoothness throughout these process cycles, as confirmed by atomic force microscopy (AFM) characterization (Supporting Information, Figure S1). Accordingly, they can be recycled for subsequent CVD growths, typically up to 20 times, offering high sustainability. Also, we emphasize that the entire process is conducted in water without involving any other chemical etchants or polymeric adhesives, thus it is intrinsically free of any chemical-driven properties degradation.

Figure 2 demonstrates the successful CVD growth and delamination of VA-2D MoS_2 layers using NaCl substrates, which were obtained by the growth recipe developed for SiO_2/Si substrates in our lab.[28,42,46] Figure 2a presents photographs of a sample taken at each preparation stage and Figure 2b depicts time-lapsed snapshot images of the corresponding 2D layers undergoing water-assisted delamination. The delamination is completed instantly after water immersion (typically within a few seconds), as presented in Supporting Information, Video 1. After this step, the delaminated 2D layers can be transferred to freshwater to ensure the complete removal of any salt ion residuals (details are described in Methods).

Figure 2c shows a low-magnification TEM image of the sample prepared in Figure 2a,b, evidencing its highly continuous film morphology without any disconnection or cracks. Figure 2d presents the corresponding selected area electron diffraction (SAED) characterization which exhibits the indexed (002) and (004) ring patterns of hexagonal MoS_2 crystals, consistent with previous observations with VA- 2D MoS_2 layers.[46,48] The HRTEM image in Figure 2e evidences that the sample is entirely composed of VA-2D MoS_2 layers, predominantly exposing their edge sites on the surface. The measured interlayer spacing is ~0.65 nm which precisely matches the (001) planar distance (that is, *c*-axis) of hexagonal MoS_2 crystals.[46,48−50] The inset in Figure 2e shows the digital micrograph intensity profile corresponding to the line-scan orientation (white arrow) in the image, confirming the uniform dimension of vdW gaps. The chemical composition of the VA-2D MoS_2 layers was characterized by energy dispersive X-ray spectroscopy (EDS). Figure 2f shows EDS profiles obtained from the same sample confirming the stoichiometric ratio of Mo/S = 1:2, which is highly consistent with previous studies.[33,51] It is remarkable to note that the EDS intensity of salt residuals is negligible, as presented in the zoomed-in image in the right panel. The chemical integrity of the sample

https://dx.doi.org/10.1021/acs.nanolett.0c01089
Nano Lett. 2020, 20, 3925−3934

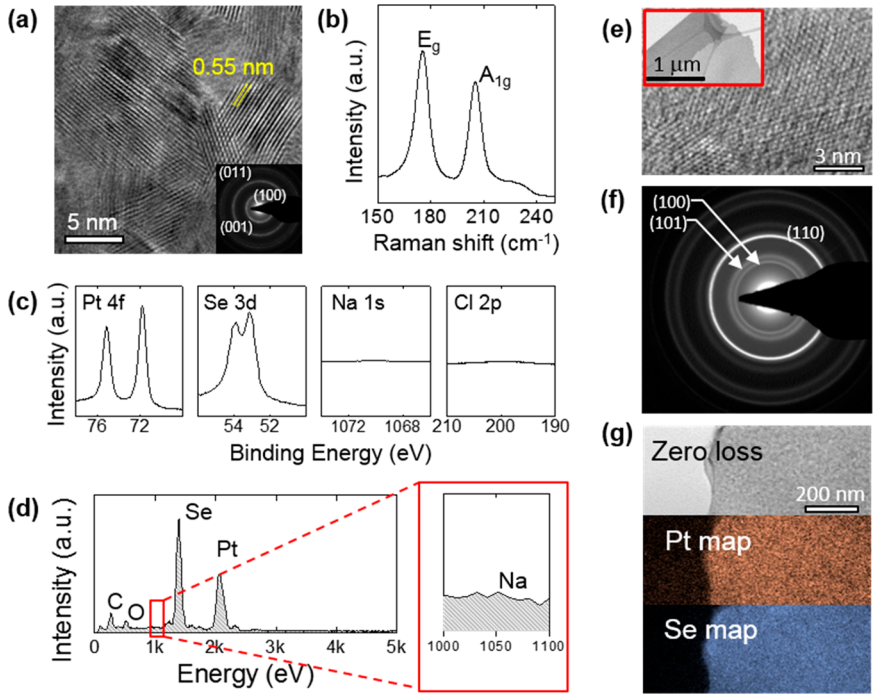

Figure 3. (a) HRTEM image of VA-2D $PtSe_2$ layers delaminated from a NaCl substrate. The inset is the corresponding SAED pattern with indexed $PtSe_2$ crystalline planes. (b) Raman spectrum, (c) XPS spectra, and (d) EDS profile obtained from the same sample of delaminated VA-2D $PtSe_2$ layers. (e) HRTEM image of HA-2D $PtSe_2$ layers delaminated from a NaCl substrate. The inset is the corresponding low-magnification TEM image. (f) SAED pattern corresponding to the sample in (e). (g) EELS elemental map images obtained from the same sample.

was further characterized by X-ray photoelectron spectroscopy (XPS). Figure 2g displays XPS core-level spectra of Mo 3d, S 2p, Na 1s, and Cl 2p binding energies obtained from the same sample. The XPS spectra of Mo 3d and S 2p reveal deconvolution peaks at the specific binding energies consistent with previous studies on 2D MoS_2 layers,[42,52,53] consistent with the SAED and EDS characterization. Meanwhile, the XPS spectra of Na 1s and Cl 2p exhibit negligible peaks, further confirming the chemically clean nature of this layer delamination approach. We note that as-delaminated 2D MoS_2 layers can exhibit a very small amount of Na^+ residuals, which can be completely removed by the additional water rinsing step described in Methods. The corresponding XPS spectra are presented in Supporting Information, Figure S2. Figure 2h presents Raman spectroscopy characterization which reveals two distinguishable peaks of in-plane E^1_{2g} and out-of-plane A_{1g} oscillation modes of 2D MoS_2 layers. It is noted that the intensity of the A_{1g} peak is significantly higher than that of the E^1_{2g} peak, which is a distinct feature of VA-2D MoS_2 layers and is fully consistent with previous studies.[42,46,54,55]

In order to verify the generality of this growth/delamination approach, we grew a variety of 2D TMD layers on diverse salt crystal substrates and delaminated them. Figure 3a–d demonstrates the CVD growth of VA-2D $PtSe_2$ layers on NaCl crystals and their water-assisted delamination. Figure 3a shows a representative HRTEM image of VA-2D $PtSe_2$ layers and their corresponding indexed SAED pattern (inset). Figure 3b presents a Raman spectroscopy profile of the same sample after delamination, revealing the E^1_{2g} and A_{1g} peaks of $PtSe_2$. Figure 3c exhibits XPS spectral profiles of Pt 4f, Se 3d, Na 1s, and Cl 2p core levels, which confirm the stoichiometric atomic ratio of $PtSe_2$.[43,56] Meanwhile, the spectral profiles of Na 1s and Cl 2p core levels do not exhibit any noticeable peaks, similar to the observation with 2D MoS_2 layers obtained from NaCl substrates. Figure 3d shows the corresponding EDS profile, which further confirms the stoichiometric ratio of Pt/Se = 1:2 with a negligible presence of Na atoms. We further extended this water-assisted growth and delamination approach to other materials, including VA-2D $PtTe_2$ layers and single-crystalline KCl substrates. The delaminated 2D layers preserve the original stoichiometry of their as-grown state,[56−58] as confirmed in Supporting Information, Figure S3. Additionally, the growth and delamination of VA-2D $PtSe_2$ layers using KCl and KBr substrates were confirmed (Supporting Information, Figures S4 and S5). The intrinsic vdW gap spacings of the VA-2D TMD layers are much smaller than the dimensions of the salts ions in their hydrated states[59] which possibly explains the negligible presence of the ions in the delaminated 2D layers. In addition to VA-2D TMD layers, HA-2D TMD layers were also grown and delaminated using salt crystals. Figure 3e–g presents a representative example of HA-2D $PtSe_2$ layers obtained from NaCl substrates. Figure 3e shows an HRTEM image of HA-2D $PtSe_2$ layers revealing the lattice fringes from their basal planes along with the corresponding low-magnification TEM image (inset). Figure 3f presents the corresponding SAED characterization obtained from a large area (>10 μm^2) of the sample exhibiting the dominant appearance of (110) diffraction ring pattern, clearly distinct from the characteristic observed with VA-2D $PtSe_2$ layers (Figure 3a inset). This observation indicates that a large number of (110) crystalline planes are orthogonally aligned with respect to the TEM beam direction, confirming that the basal planes of 2D $PtSe_2$ layers are horizontally aligned consistent with previous studies.[43,45] Figure 3g shows TEM electron energy loss spectroscopy (EELS) maps of the corresponding sample, revealing a highly uniform spatial distribution of constituent elements. Additional characterization results further verify the crystalline structure and

https://dx.doi.org/10.1021/acs.nanolett.0c01089
Nano Lett. 2020, 20, 3925−3934

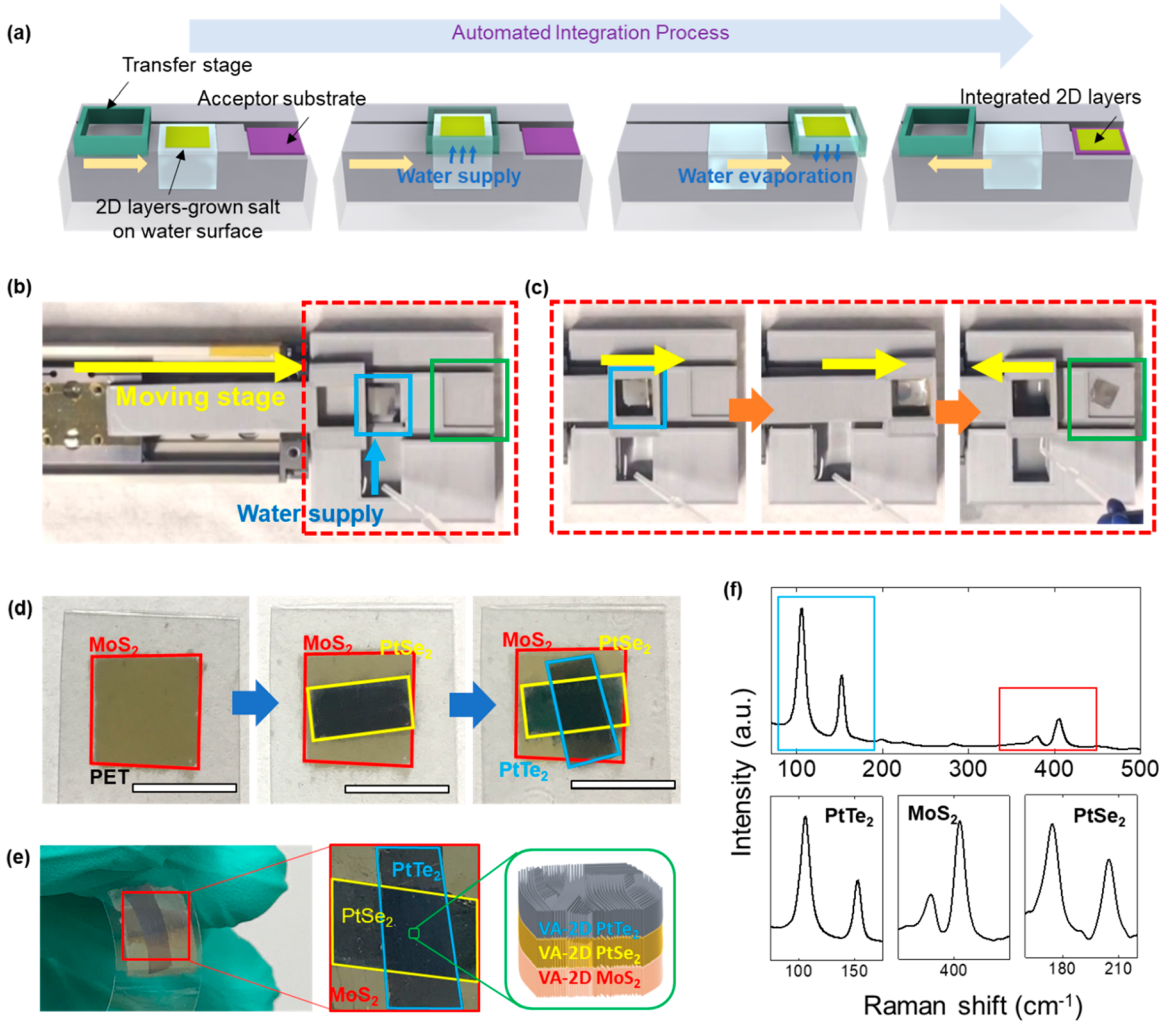

Figure 4. (a) Schematic illustration and working principle for the water-assisted automated integration of 2D TMD layers. (b) Top-to-bottom view of a home-built 2D layer integration stage describing its major components. (c) Time-lapsed snapshot images sequentially depicting the water-assisted automated integration of VA-2D $PtTe_2$ layers. (d) Heterogeneous integration of three-different VA-2D TMD layers on a PET substrate. The scale bar is 1 cm. (e) Mechanical flexibility of VA-2D TMD heterolayers. The sample is different from that in (d). (f) Raman spectral profiles obtained from a sample of 2D heterolayers composed of $PtTe_2$, MoS_2, and $PtSe_2$.

stoichiometric composition of the delaminated HA-2D $PtSe_2$ layers (Supporting Information, Figures S6 and S7).

We then demonstrated the heterogeneous integration of multiple VA-2D TMD layers on unconventional substrates, achieving 2D/2D heterolayers. To this end, we developed a home-built stage which enables the layer-by-layer delamination and integration of various 2D TMD layers in an "automated" manner. Figure 4a shows a schematic illustration of the apparatus describing its working principle. It is composed of three major components; (1) loading stage where as-grown 2D TMD/salt substrate samples are loaded, (2) water chamber which supplies a controlled amount of water to the loading stage, and (3) integration stage where delaminated 2D TMD layers are individually stacked up. Figure 4b shows a top-to-bottom view of the home-built apparatus specifying the loading stage (blue box) containing a sample of VA-2D $PtTe_2$/NaCl substrate and the integration stage (green box). The blue arrow presents the flow of water into the sample stage and the yellow arrow denotes the movement of the loading rod, both of which are executed in a fully automated manner. Figure 4c specifies the 2D layer integration event occurring in the red dotted box in Figure 4b in a time-lapsed manner. Once the VA-2D $PtTe_2$ layers are delaminated within the blue-boxed sample stage (left panel), they are subsequently transferred to the integration stage by the loading rod (middle panel). Eventually, they become integrated onto the preloaded target substrate within the green boxed stage and the loading rod returns to the starting point for the next processes (right panel). Mild heating can be optionally applied to the integration stage to promote the evaporation of the supplied water to ensure the robust integration of each sample. The video file corresponding to the procedures described in Figure 4c is presented in Supporting Information, Video 2. We demonstrated the integration of wafer-scale 2D TMD heterolayers employing various components of controlled orientation. Figure 4d shows representative images demonstrating the sequential integration of three different VA-2D TMD layers, that is, MoS_2, $PtSe_2$, and $PtTe_2$, on top of a polyethylene terephthalate (PET) substrate (purchased from Eg-eMigoo). The lateral dimension of each material is greater than a few square centimenters, and the $PtSe_2$ and $PtTe_2$ layers were intentionally grown to be in rectangular shapes for better visualization. Figure 4e presents another example of large-area $PtTe_2/PtSe_2/MoS_2$ heterolayers integrated on a mechanically

https://dx.doi.org/10.1021/acs.nanolett.0c01089
Nano Lett. 2020, 20, 3925−3934

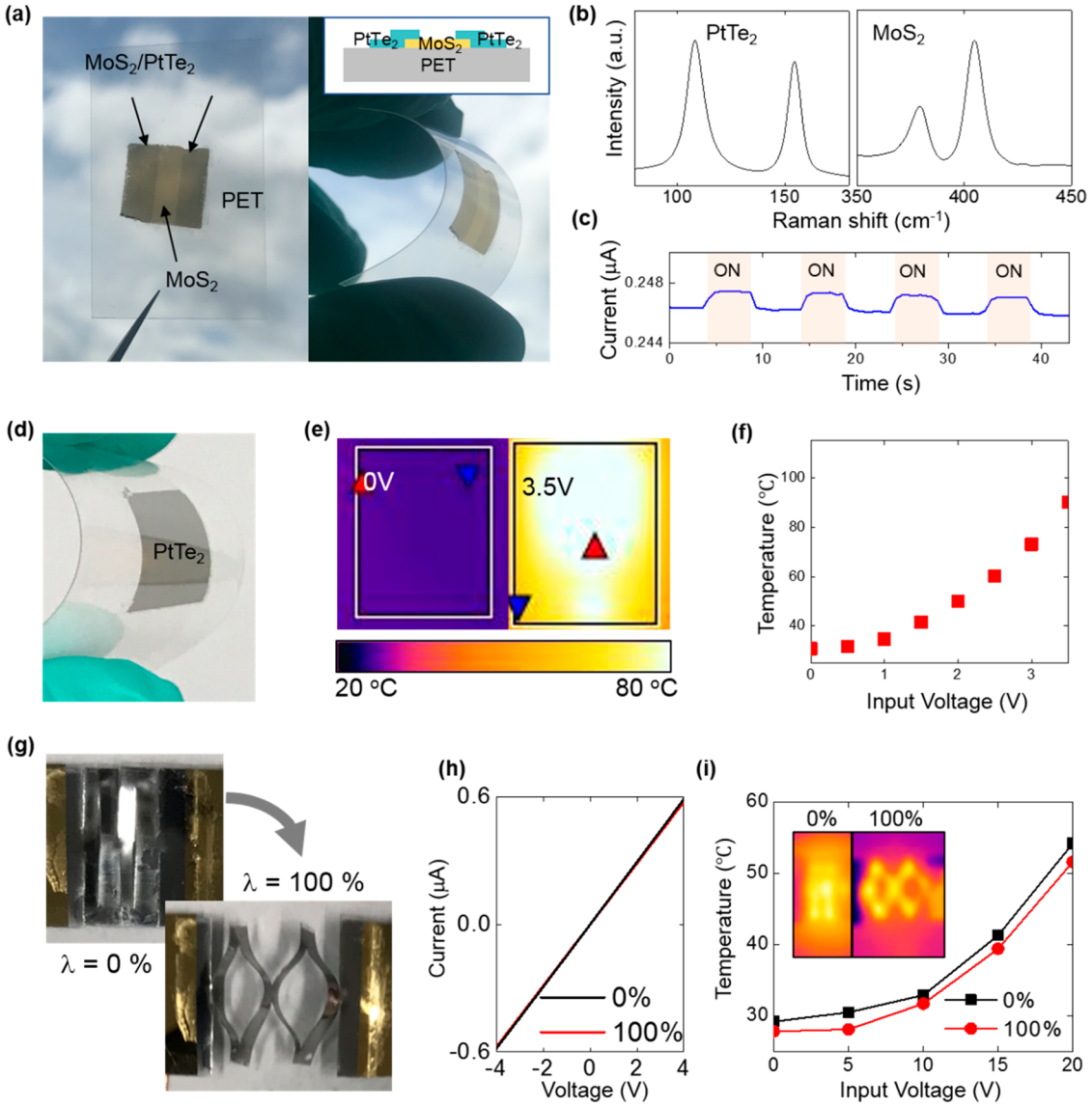

Figure 5. (a) Large area all 2D heterolayers composed of VA-2D $PtTe_2$ layers partially interfacing with VA-2D MoS_2 layers integrated on a PET substrate. The inset image on the right panel demonstrates that VA-2D $PtTe_2$ layers function as metallic electrodes for semiconducting VA-2D MoS_2 layers. (b) Raman profiles obtained from the same sample, zooming in the wavenumber ranges specific to $PtTe_2$ and MoS_2. (c) Demonstration of photoresponsiveness with the same sample upon a periodic illumination of a white light. (d) VA-2D $PtTe_2$ layers integrated on a PET substrate. (e) IR images of the sample in (d) obtained at a bias of 0 and 3.5 V. (f) Electro-thermal performance of the same sample presenting a plot of voltage versus temperature. (g) Images of kirigami-patterned VA-2D $PtTe_2$ layers on a PI substrate under 0% and 100% strain. (h) $I-V$ characteristics obtained from the same kirigami sample revealing strain-invariant electrical properties. (i) Plot of voltage versus temperature obtained from the same kirigami sample under 0% and 100% strain. The inset shows IR images of the same sample obtained at a bias of 20 V.

bendable substrate maintaining their vertical alignment. We also demonstrated other heterolayers stacked in a different order, that is, $PtSe_2/MoS_2/PtTe_2$ (Supporting Information, Figure S8), confirming the high controllability of layer stacking order. The chemical integrity of these large-area 2D heterolayers was characterized by Raman spectroscopy, as shown in Figure 4f. The image on the top panel shows a Raman spectrum obtained from a stacked region of $PtTe_2/MoS_2$. The $PtTe_2$ and MoS_2 Raman spectra presented on the bottom panel correspond to the enlarged views of the blue and red boxed regions on the top panel, respectively. The $PtSe_2$ Raman spectrum on the bottom panel was separately obtained from a region containing only 2D $PtSe_2$ layers. The corresponding XPS profiles obtained from the stacked region of $PtTe_2/MoS_2$ are presented in Supporting Information, Figure S9.

Finally, we studied opportunities of this 2D layer delamination/integration approach for unconventional device applications difficult to achieve with any other methods, that is, large-area "all 2D" layers-enabled photodetection (Figure 5a–c) and mechanically reconfigurable electro-thermal heaters (Figure 5d–i). For all 2D photodetection, we employed $MoS_2/PtTe_2$ heterolayers integrated on a flexible PET substrate (Figure 5a), prepared by the sequential growth of individual 2D layer components and their delamination as described in Supporting Information, Figure S10. In this sample configuration, two separate 2D $PtTe_2$ layers are partially interfaced with the two ends of 2D MoS_2 layers, as shown in the schematic illustration on the right panel. Given

https://dx.doi.org/10.1021/acs.nanolett.0c01089
Nano Lett. 2020, 20, 3925−3934

their intrinsically metallic nature with extremely high electrical conductivities, that is, $>10^6$ S/m,[57,60,61] the integrated 2D $PtTe_2$ layers function as near atom-thickness metallic electrodes for the semiconducting 2D MoS_2 layers. Figure 5b presents the Raman spectral profiles of the sample obtained from the wavenumber ranges specific to $PtTe_2$-only and MoS_2-only. Figure 5c shows a periodic generation of photocurrent upon a cyclic illumination of visible light onto the sample. The results confirm a demonstration of large-area "all 2D" photoresponsive TMD heterolayers where both photoactive media and contact electrodes are 2D layers. As another example of unconventional electronic devices, we studied electro-thermal applications of large-area 2D $PtTe_2$ layers integrated on a PET substrate (Figure 5d). We studied the Joule heating responsiveness of the 2D $PtTe_2$/PET sample by characterizing its infrared (IR) images under electrical biasing. Figure 5e shows IR images of the 2D $PtTe_2$ layers taken at a bias of 0 and 3.5 V, visualizing a drastic change of bias-dependent temperature. Figure 5f shows a plot of applied voltage versus resulting temperature obtained from the same sample, confirming a substantial Joule heating effect. Indeed, the measured electro-thermal efficiency, that is, temperature increase per applied voltage, is significantly higher than those observed with other metallic nanomaterials including graphene, carbon nanotubes, and silver nanowires.[62−64] We further explored this opportunity and developed 2D $PtTe_2$ layer-based mechanically reconfigurable electrically driven heaters. For this, we integrated 2D $PtTe_2$ layers on polyamide (PI) substrates (purchased from ColePalmer) with higher thermal stability as the PET substrates were more prone to Joule-heating driven deformation (Supporting Information, Figure S11). We then created kirigami cuts on the 2D $PtTe_2$ layers/PI samples to ensure a large degree of mechanical stretchability.[22,43] Figure 5g shows images of a kirigami-patterned 2D $PtTe_2$/PI sample at 0% and 100% strain rate λ which is defined to be $\Delta L/L_o$ where ΔL denotes the increase of lateral length with respect to the original length L_o. Details for the kirigami pattern dimensions are presented in Supporting Information, Figure S12. The sample exhibits strain-invariant conductance even up to 100% strain, as shown by the $I-V$ characteristics in Figure 5h. We then studied the electro-thermal responsiveness of this stretchable kirigami sample, and Figure 5i presents a plot of temperature versus voltage before and after lateral stretching. The sample exhibits an insignificant drop of bias-driven heating even up to 100% strain, as also manifested by the corresponding IR images presented in the inset. All these proof-of-concept demonstrations emphasize the high versatility of integrating 2D TMD layers of controlled chemistry and morphology onto functional substrates in realizing futuristic device applications.

CONCLUSION

We report a new method to heterogeneously integrate wafer-scale 2D TMD layers onto secondary substrates in a highly scalable and controllable manner. We employed salt crystals as growth substrates, which enable water-assisted delamination of as-grown 2D TMD layers irrespective of their compositions and orientations. We demonstrated a fully automated assembly of wafer-scale 2D TMD layers on unconventional substrates difficult with other approaches. These wafer-scale 2D TMD heterolayers retaining their intrinsic material properties enable a variety of near atom-thickness device building blocks of diverse form factors.

METHODS

Growth of 2D TMD Layers. CVD was performed for the sulfurization, selenization, and tellurization of predeposited metals using a horizontal quartz tube furnace (Lindberg/Blue M Mini-Mite). Metal films of various thicknesses were deposited on single-crystalline salt substrates (TedPella, 99% single crystal) by an electron beam evaporator (Temescal) at a deposition rate of 0.1 Å/s, that is, 0.7 nm Pt for HA- 2D $PtSe_2$ layers, 1.5 nm Pt for HA-2D $PtTe_2$ layers, and 6 nm Pt and Mo for VA-2D $PtSe_2$, VA-2D $PtTe_2$, and VA-2D MoS_2. The metal-deposited salt crystals were placed in the center zone of the CVD furnace. Alumina boats containing chalcogenide powders specific to targeted 2D TMD layers were placed in the upstream side of the furnace, that is, Se and Te for $PtSe_2$ and $PtTe_2$, respectively, and S for MoS_2. All the chalcogen powders were high purity (∼99.9%) and were purchased from MilliporeSigma. The quartz tube was pumped down to a base pressure of ∼20 mTorr and purged with Ar gas for ∼10 min to remove organic residuals in it. Subsequently, it was heated to the reaction temperature specific to target materials, that is, 400 °C for 2D $PtSe_2$ and 2D $PtTe_2$ layers and 550 °C for MoS_2. The total ramping time was 50 min, and the reaction was maintained at the target temperature for another 50 min. Throughout the reaction, Ar gas was supplied at a constant rate of 100 standard cubic centimeters per minute, and the furnace was naturally cooled down to room temperature once the reaction was over. Prior to the metal deposition, as-purchased salt crystals can be optionally polished with polishing papers (purchased from Micro-Surface) without applying liquid if their surface smoothness needs to be improved; initial rough polishing was with 4000 grit and final fine polishing was with 12000 grit.

Delamination and Integration of 2D TMD Layers. For the manual transfer of 2D TMD layers, as-prepared samples are immersed in DI water until their complete delamination. The delaminated 2D layers floating on the water surface are maintained at 70 °C, followed by a subsequent transfer to fresh DI water to remove any residual salt elements. The 2D TMDs layers integrated on secondary substrates are dried on a hot plate at 70 °C for ∼12 h to remove residual water. For the demonstration of the water-assisted automated integration of 2D TMD layers, we fabricated the setup and the loading rod presented in Figure 4b using a 3D printer (PRUSA i3MK3). The loading rod was manually connected to a home-built tensile stretcher, which moves it between the sample stage and the integration stage in an automated manner.

Structural and Chemical Characterization. TEM characterization was performed using JEOL ARM 200F Cs-corrected TEM and FEI F30 TEM at an accelerating voltage of 200 and 300 kV, respectively. Raman characterization was using Renishaw RM 1000B system with a laser source of 514 nm wavelength. XPS characterization was performed using ESCALAB 250 with an Al Kα-ray source (1486.3 eV) in ultrahigh vacuum condition (10^{-9} mBar)

Device Fabrication and Electrical Measurement. For electrical measurements, Au (70 nm thickness) electrodes were deposited on top of the 2D $PtTe_2$ layers interfaced with 2D MoS_2 layers (Figure 5a) or integrated on PET (Figure 5d) through a shadow mask. Two-terminal electrical measurements were performed using a home-built probe station connected with a semiconductor parameter analyzer (HP 4156A). Photoresponsiveness measurements (Figure 5c) were per-

https://dx.doi.org/10.1021/acs.nanolett.0c01089
Nano Lett. 2020, 20, 3925−3934

formed using a white LED with a power intensity of 164 W/m^2 at 1 V.

■ ASSOCIATED CONTENT

Supporting Information

The Supporting Information is available free of charge at https://pubs.acs.org/doi/10.1021/acs.nanolett.0c01089.

AFM, optical images of samples, XPS data, TEM/EDS data (PDF)

Video of layers undergoing water-assisted delamination that is completed instantly after water immersion (MP4)

Video of mild heating applied to integration stage to promote the evaporation of supplied water (MP4)

■ AUTHOR INFORMATION

Corresponding Author

Yeonwoong Jung − *NanoScience Technology Center and Department of Materials Science and Engineering, University of Central Florida, Orlando, Florida 32826, United States; Analytical Research Division, Korea Basic Science Institute, Jeonju 54907, South Korea;* orcid.org/0000-0001-6042-5551; Email: Yeonwoong.Jung@ucf.edu

Authors

Sang Sub Han − *NanoScience Technology Center, University of Central Florida, Orlando, Florida 32826, United States; Department of Material Science and Engineering, Seoul National University, Seoul 08826, South Korea*

Tae-Jun Ko − *NanoScience Technology Center, University of Central Florida, Orlando, Florida 32826, United States*

Changhyeon Yoo − *NanoScience Technology Center, University of Central Florida, Orlando, Florida 32826, United States*

Mashiyat Sumaiya Shawkat − *NanoScience Technology Center and Department of Electrical and Computer Engineering, University of Central Florida, Orlando, Florida 32826, United States;* orcid.org/0000-0001-6594-190X

Hao Li − *NanoScience Technology Center and Department of Materials Science and Engineering, University of Central Florida, Orlando, Florida 32826, United States*

Bo Kyung Kim − *Analytical Research Division, Korea Basic Science Institute, Jeonju 54907, South Korea*

Woong-Ki Hong − *Analytical Research Division, Korea Basic Science Institute, Jeonju 54907, South Korea;* orcid.org/0000-0001-8221-1028

Tae-Sung Bae − *Analytical Research Division, Korea Basic Science Institute, Jeonju 54907, South Korea*

Hee-Suk Chung − *Analytical Research Division, Korea Basic Science Institute, Jeonju 54907, South Korea*

Kyu Hwan Oh − *Department of Material Science and Engineering, Seoul National University, Seoul 08826, South Korea*

Complete contact information is available at: https://pubs.acs.org/10.1021/acs.nanolett.0c01089

Author Contributions

S.S.H. conceived the project idea under the guidance of Y.J. S.S.H. prepared the 2D TMD layer samples including their CVD growth and water-assisted delamination. T.-J.K. and C.Y. participated in preparing the samples and developing the automated stage for the integration of 2D layers. M.S.S. participated in the electrical characterization of the samples. H.L. participated in preparing the samples and writing the manuscript. S.S.H., B.K.K., W.-K.H., T.-S.B., and H.-S.C. performed the structural characterization including TEM, Raman, and XPS under the guidance of K.H.O. and Y.J. S.S.H., H.L., and Y.J. wrote the manuscript with input from all authors.

Notes

The authors declare no competing financial interest.

■ ACKNOWLEDGMENTS

This work was supported by the National Science Foundation (CMMI-1728390) (M.S.S., and Y.J.), the Korea Institute of Energy Technology Evaluation and Planning (KETEP) and the Ministry of Trade, Industry, & Energy (MOTIE) of the Republic of Korea (No. 20173010013340) (Y.J.). Y.J. also acknowledges VPR Advancement of Early Career Researchers award from the University of Central Florida. This research was in part supported by the Creative Materials Discovery Program through the National Research Foundation of Korea (NRF) funded by the Ministry of Science, ICT, and Future Planning (NRF-2017M3D1A1039553). H.S.C. was supported by the National Research Foundation of Korea (NRF) grant funded by the Korea government (MSIT) (No. 2019R1F1A1058410). We also acknowledge the National Science Foundation (MRI XPS: ECCS:1726636) for the XPS characterization. This research was a part of the project titled "Development of cleanup technology for spilled oil and floating HNS using nanostructured structures", funded by the Korea Coast Guard of the Korean government. K.H.O. also acknowledges support through a Grant (KCG-01-2017-02) titled "Development of cleanup technology for spilled oil and foating HNS using nanostructures" by the Korea Coast Guard.

■ REFERENCES

(1) Zhu, J.; Dexheimer, M.; Cheng, H. Reconfigurable Systems for Multifunctional Electronics. *npj Flexible Electronics* **2017**, *1* (1), 8−20.

(2) Kang, P.; Kim, K. H.; Park, H. G.; Nam, S. Mechanically Reconfigurable Architectured Graphene for Tunable Plasmonic Resonances. *Light: Sci. Appl.* **2018**, *7*, 17−25.

(3) Kabiri Ameri, S.; Ho, R.; Jang, H.; Tao, L.; Wang, Y.; Wang, L.; Schnyer, D. M.; Akinwande, D.; Lu, N. Graphene Electronic Tattoo Sensors. *ACS Nano* **2017**, *11* (8), 7634−7641.

(4) Tan, C.; Cao, X.; Wu, X.-J.; He, Q.; Yang, J.; Zhang, X.; Chen, J.; Zhao, W.; Han, S.; Nam, G.-H.; Sindoro, M.; Zhang, H. Recent Advances in Ultrathin Two-Dimensional Nanomaterials. *Chem. Rev.* **2017**, *117* (9), 6225−6331.

(5) Zhang, H. Ultrathin Two-Dimensional Nanomaterials. *ACS Nano* **2015**, *9* (10), 9451−9469.

(6) Gao, L. Flexible Device Applications of 2D Semiconductors. *Small* **2017**, *13* (35), 1603994−1604018.

(7) Choi, W.; Choudhary, N.; Han, G. H.; Park, J.; Akinwande, D.; Lee, Y. H. Recent Development of Two-Dimensional Transition Metal Dichalcogenides and Their Applications. *Mater. Today* **2017**, *20* (3), 116−130.

(8) Ferrari, A. C.; Bonaccorso, F.; Fal'ko, V.; Novoselov, K. S.; Roche, S.; Bøggild, P.; Borini, S.; Koppens, F. H. L.; Palermo, V.; Pugno, N.; Garrido, J. A.; Sordan, R.; Bianco, A.; Ballerini, L.; Prato, M.; Lidorikis, E.; Kivioja, J.; Marinelli, C.; Ryhanen, T.; Morpurgo, A.; Coleman, J. N.; Nicolosi, V.; Colombo, L.; Fert, A.; Garcia-Hernandez, M.; Bachtold, A.; Schneider, G. F.; Guinea, F.; Dekker, C.; Barbone, M.; Sun, Z.; Galiotis, C.; Grigorenko, A. N.; Konstantatos, G.; Kis, A.; Katsnelson, M.; Vandersypen, L.; Loiseau, A.; Morandi, V.; Neumaier, D.; Treossi, E.; Pellegrini, V.; Polini, M.; Tredicucci, A.; Williams, G. M.; Hee Hong, B.; Ahn, J.-H.; Min Kim, J.; Zirath, H.; van Wees, B. J.; van der Zant, H.; Occhipinti, L.; Di Matteo, A.; Kinloch, I. A.; Seyller, T.; Quesnel, E.; Feng, X.; Teo, K.;

Rupesinghe, N.; Hakonen, P.; Neil, S. R. T.; Tannock, Q.; Lofwander, T.; Kinaret, J. Science and Technology Roadmap for Graphene, Related Two-Dimensional Crystals, and Hybrid Systems. *Nanoscale* **2015**, *7* (11), 4598−4810.
(9) Li, Y.; Wang, Y.; Huang, L.; Wang, X.; Li, X.; Deng, H. X.; Wei, Z.; Li, J. Anti-Ambipolar Field-Effect Transistors Based On Few-Layer 2D Transition Metal Dichalcogenides. *ACS Appl. Mater. Interfaces* **2016**, *8* (24), 15574−81.
(10) Duan, X.; Wang, C.; Pan, A.; Yu, R.; Duan, X. Two-Dimensional Transition Metal Dichalcogenides as Atomically Thin Semiconductors: Opportunities and Challenges. *Chem. Soc. Rev.* **2015**, *44* (24), 8859−8876.
(11) Novoselov, K. S.; Mishchenko, A.; Carvalho, A.; Castro Neto, A. H. 2D Materials and Van der Waals Heterostructures. *Science* **2016**, *353* (6298), aac9439.
(12) Bao, X.; Ou, Q.; Xu, Z.-Q.; Zhang, Y.; Bao, Q.; Zhang, H. Band Structure Engineering in 2D Materials for Optoelectronic Applications. *Advanced Materials Technologies* **2018**, *3* (11), 1800072−1800085.
(13) Duan, X.; Wang, C.; Fan, Z.; Hao, G.; Kou, L.; Halim, U.; Li, H.; Wu, X.; Wang, Y.; Jiang, J.; Pan, A.; Huang, Y.; Yu, R.; Duan, X. Synthesis of $WS_{2x}Se_{2-2x}$ Alloy Nanosheets with Composition-Tunable Electronic Properties. *Nano Lett.* **2016**, *16* (1), 264−269.
(14) Cheng, R.; Li, D.; Zhou, H.; Wang, C.; Yin, A.; Jiang, S.; Liu, Y.; Chen, Y.; Huang, Y.; Duan, X. Electroluminescence and Photocurrent Generation from Atomically Sharp WSe_2/MoS_2 Heterojunction p-n Diodes. *Nano Lett.* **2014**, *14* (10), 5590−5597.
(15) Mann, J.; Ma, Q.; Odenthal, P. M.; Isarraraz, M.; Le, D.; Preciado, E.; Barroso, D.; Yamaguchi, K.; von Son Palacio, G.; Nguyen, A.; Tran, T.; Wurch, M.; Nguyen, A.; Klee, V.; Bobek, S.; Sun, D.; Heinz, T. F.; Rahman, T. S.; Kawakami, R.; Bartels, L. 2-Dimensional Transition Metal Dichalcogenides with Tunable Direct Band Gaps: $MoS_{2(1-x)}Se_{2x}$ Monolayers. *Adv. Mater.* **2014**, *26* (9), 1399−1404.
(16) Li, H.; Duan, X.; Wu, X.; Zhuang, X.; Zhou, H.; Zhang, Q.; Zhu, X.; Hu, W.; Ren, P.; Guo, P.; Ma, L.; Fan, X.; Wang, X.; Xu, J.; Pan, A.; Duan, X. Growth of Alloy $MoS_{2x}Se_{2(1-x)}$ Nanosheets with Fully Tunable Chemical Compositions and Optical Properties. *J. Am. Chem. Soc.* **2014**, *136* (10), 3756−3759.
(17) Furchi, M. M.; Pospischil, A.; Libisch, F.; Burgdörfer, J.; Mueller, T. Photovoltaic Effect in an Electrically Tunable van der Waals Heterojunction. *Nano Lett.* **2014**, *14* (8), 4785−4791.
(18) Gong, Y.; Lin, J.; Wang, X.; Shi, G.; Lei, S.; Lin, Z.; Zou, X.; Ye, G.; Vajtai, R.; Yakobson, B. I.; Terrones, H.; Terrones, M.; Tay, B. K.; Lou, J.; Pantelides, S. T.; Liu, Z.; Zhou, W.; Ajayan, P. M. Vertical and In-Plane Heterostructures from WS_2/MoS_2 Monolayers. *Nat. Mater.* **2014**, *13*, 1135−1155.
(19) Wang, Q. H.; Kalantar-Zadeh, K.; Kis, A.; Coleman, J. N.; Strano, M. S. Electronics and Optoelectronics of Two-Dimensional Transition Metal Dichalcogenides. *Nat. Nanotechnol.* **2012**, *7* (11), 699−712.
(20) Butler, S. Z.; Hollen, S. M.; Cao, L.; Cui, Y.; Gupta, J. A.; Gutierrez, H. R.; Heinz, T. F.; Hong, S. S.; Huang, J.; Ismach, A. F.; Johnston-Halperin, E.; Kuno, M.; Plashnitsa, V. V.; Robinson, R. D.; Ruoff, R. S.; Salahuddin, S.; Shan, J.; Shi, L.; Spencer, M. G.; Terrones, M.; Windl, W.; Goldberger, J. E. Progress, Challenges, and Opportunities in Two-Dimensional Materials beyond Graphene. *ACS Nano* **2013**, *7* (4), 2898−2926.
(21) Radisavljevic, B.; Radenovic, A.; Brivio, J.; Giacometti, V.; Kis, A. Single-Layer MoS_2 Transistors. *Nat. Nanotechnol.* **2011**, *6* (3), 147−150.
(22) Akinwande, D.; Brennan, C. J.; Bunch, J. S.; Egberts, P.; Felts, J. R.; Gao, H.; Huang, R.; Kim, J.-S.; Li, T.; Li, Y.; Liechti, K. M.; Lu, N.; Park, H. S.; Reed, E. J.; Wang, P.; Yakobson, B. I.; Zhang, T.; Zhang, Y.-W.; Zhou, Y.; Zhu, Y. A Review on Mechanics and Mechanical Properties of 2D Materials—Graphene and Beyond. *Extreme Mechanics Letters* **2017**, *13*, 42−77.
(23) Mak, K. F.; Shan, J. Photonics and Optoelectronics of 2D Semiconductor Transition Metal Dichalcogenides. *Nat. Photonics* **2016**, *10* (4), 216−226.
(24) Cho, B.; Yoon, J.; Lim, S. K.; Kim, A. R.; Kim, D.-H.; Park, S.-G.; Kwon, J.-D.; Lee, Y.-J.; Lee, K.-H.; Lee, B. H.; Ko, H. C.; Hahm, M. G. Chemical sensing of 2D graphene/MoS_2 heterostructure device. *ACS Appl. Mater. Interfaces* **2015**, *7* (30), 16775−16780.
(25) Xu, M.; Liang, T.; Shi, M.; Chen, H. Graphene-like Two-Dimensional Materials. *Chem. Rev.* **2013**, *113* (5), 3766−3798.
(26) Moving Towards The Market. *Nat. Mater.*, **2019**, *18*(6) 519−519.
(27) Masubuchi, S.; Morimoto, M.; Morikawa, S.; Onodera, M.; Asakawa, Y.; Watanabe, K.; Taniguchi, T.; Machida, T. Autonomous Robotic Searching and Assembly of Two-Dimensional Crystals to Build Van der Waals Superlattices. *Nat. Commun.* **2018**, *9* (1), 1413−1424.
(28) Choudhary, N.; Park, J.; Hwang, J. Y.; Chung, H.-S.; Dumas, K. H.; Khondaker, S. I.; Choi, W.; Jung, Y. Centimeter Scale Patterned Growth of Vertically Stacked Few Layer Only 2D MoS_2/WS_2 Van der Waals Heterostructure. *Sci. Rep.* **2016**, *6*, 25456−25462.
(29) Geim, A. K.; Grigorieva, I. V. Van der Waals Heterostructures. *Nature* **2013**, *499*, 419−425.
(30) Lee, C.-H.; Lee, G.-H.; van der Zande, A. M.; Chen, W.; Li, Y.; Han, M.; Cui, X.; Arefe, G.; Nuckolls, C.; Heinz, T. F.; Guo, J.; Hone, J.; Kim, P. Atomically Thin p-n Junctions with Van der Waals Heterointerfaces. *Nat. Nanotechnol.* **2014**, *9*, 676−681.
(31) Bonaccorso, F.; Lombardo, A.; Hasan, T.; Sun, Z.; Colombo, L.; Ferrari, A. C. Production and Processing of graphene and 2D Crystals. *Mater. Today* **2012**, *15* (12), 564−589.
(32) Kang, K.; Lee, K. H.; Han, Y.; Gao, H.; Xie, S.; Muller, D. A.; Park, J. Layer-By-Layer Assembly of Two-Dimensional Materials into Wafer-Scale Heterostructures. *Nature* **2017**, *550* (7675), 229−233.
(33) Kim, J. H.; Ko, T. J.; Okogbue, E.; Han, S. S.; Shawkat, M. S.; Kaium, M. G.; Oh, K. H.; Chung, H. S.; Jung, Y. Centimeter-scale Green Integration of Layer-by-Layer 2D TMD vdW Heterostructures on Arbitrary Substrates by Water-Assisted Layer Transfer. *Sci. Rep.* **2019**, *9* (1), 1641−1650.
(34) Zhang, F.; Erb, C.; Runkle, L.; Zhang, X.; Alem, N. Etchant-Free Transfer of 2D Nanostructures. *Nanotechnology* **2018**, *29* (2), 025602−025607.
(35) Islam, M. A.; Kim, J. H.; Schropp, A.; Kalita, H.; Choudhary, N.; Weitzman, D.; Khondaker, S. I.; Oh, K. H.; Roy, T.; Chung, H. S.; Jung, Y. Centimeter-Scale 2D van der Waals Vertical Heterostructures Integrated on Deformable Substrates Enabled by Gold Sacrificial Layer-Assisted Growth. *Nano Lett.* **2017**, *17* (10), 6157−6165.
(36) Gurarslan, A.; Yu, Y.; Su, L.; Yu, Y.; Suarez, F.; Yao, S.; Zhu, Y.; Ozturk, M.; Zhang, Y.; Cao, L. Surface-Energy-Assisted Perfect Transfer of Centimeter-Scale Monolayer and Few-Layer MoS_2 Films onto Arbitrary Substrates. *ACS Nano* **2014**, *8* (11), 11522−11528.
(37) Zhang, L.; Wang, C.; Liu, X. L.; Xu, T.; Long, M.; Liu, E.; Pan, C.; Su, G.; Zeng, J.; Fu, Y.; Wang, Y.; Yan, Z.; Gao, A.; Xu, K.; Tan, P. H.; Sun, L.; Wang, Z.; Cui, X.; Miao, F. Damage-Free and Rapid Transfer of CVD-Grown Two-Dimensional Transition Metal Dichalcogenides by Dissolving Sacrificial Water-Soluble Layers. *Nanoscale* **2017**, *9* (48), 19124−19130.
(38) Lee, C. H.; McCulloch, W.; Lee, E. W.; Ma, L.; Krishnamoorthy, S.; Hwang, J.; Wu, Y.; Rajan, S. Transferred Large Area Single Crystal MoS_2 Field Effect Transistors. *Appl. Phys. Lett.* **2015**, *107* (19), 193503−193507.
(39) Jin, G.; Lee, C.-S.; Liao, X.; Kim, J.; Wang, Z.; Okello, O. F. N.; Park, B.; Park, J.; Han, C.; Heo, H.; Kim, J.; Oh, S. H.; Choi, S.-Y.; Park, H.; Jo, M.-H. Atomically Thin Three-Dimensional Membranes of Van der Waals Semiconductors by Wafer-Scale Growth. *Science Advances* **2019**, *5* (7), No. eaaw3180.
(40) Hwang, J.-H.; Islam, M. A.; Choi, H.; Ko, T.-J.; Rodriguez, K. L.; Chung, H.-S.; Jung, Y.; Lee, W. H. Improving Electrochemical Pb^{2+} Detection Using a Vertically Aligned 2D MoS_2 Nanofilm. *Anal. Chem.* **2019**, *91* (18), 11770−11777.

https://dx.doi.org/10.1021/acs.nanolett.0c01089
Nano Lett. 2020, 20, 3925−3934

(41) Islam, M. A.; Kim, J. H.; Ko, T.-J.; Noh, C.; Nehate, S.; Kaium, M. G.; Ko, M.; Fox, D.; Zhai, L.; Cho, C.-H.; Sundaram, K. B.; Bae, T.-S.; Jung, Y.; Chung, H.-S.; Jung, Y. Three dimensionally-ordered 2D MoS_2 vertical layers integrated on flexible substrates with stretch-tunable functionality and improved sensing capability. *Nanoscale* **2018**, *10* (37), 17525−17533.
(42) Islam, M. A.; Church, J.; Han, C.; Chung, H. S.; Ji, E.; Kim, J. H.; Choudhary, N.; Lee, G. H.; Lee, W. H.; Jung, Y. Noble Metal-Coated MoS_2 Nanofilms with Vertically-Aligned 2D Layers for Visible Light-Driven Photocatalytic Degradation of Emerging Water Contaminants. *Sci. Rep.* **2017**, *7* (1), 14944−14953.
(43) Okogbue, E.; Han, S. S.; Ko, T. J.; Chung, H. S.; Ma, J.; Shawkat, M. S.; Kim, J. H.; Kim, J. H.; Ji, E.; Oh, K. H.; Zhai, L.; Lee, G. H.; Jung, Y. Multifunctional Two-Dimensional $PtSe_2$-Layer Kirigami Conductors with 2000% Stretchability and Metallic-to-Semiconducting Tunability. *Nano Lett.* **2019**, *19*, 7598−7607.
(44) Okogbue, E.; Kim, J. H.; Ko, T. J.; Chung, H. S.; Krishnaprasad, A.; Flores, J. C.; Nehate, S.; Kaium, M. G.; Park, J. B.; Lee, S. J.; Sundaram, K. B.; Zhai, L.; Roy, T.; Jung, Y. Centimeter-Scale Periodically Corrugated Few-Layer 2D MoS_2 with Tensile Stretch-Driven Tunable Multifunctionalities. *ACS Appl. Mater. Interfaces* **2018**, *10* (36), 30623−30630.
(45) Han, S. S.; Kim, J. H.; Noh, C.; Kim, J. H.; Ji, E.; Kwon, J.; Yu, S. M.; Ko, T. J.; Okogbue, E.; Oh, K. H.; Chung, H. S.; Jung, Y.; Lee, G. H.; Jung, Y. Horizontal-to-Vertical Transition of 2D Layer Orientation in Low-Temperature Chemical Vapor Deposition-Grown $PtSe_2$ and Its Influences on Electrical Properties and Device Applications. *ACS Appl. Mater. Interfaces* **2019**, *11* (14), 13598−13607.
(46) Jung, Y.; Shen, J.; Liu, Y.; Woods, J. M.; Sun, Y.; Cha, J. J. Metal seed layer thickness-induced transition from vertical to horizontal growth of MoS_2 and WS_2. *Nano Lett.* **2014**, *14* (12), 6842−6849.
(47) Van Artsdalen, E. R.; Yaffe, I. S. Electrical Conductance and Density of Molten Salt Systems: KCl-LiCl, KCl-NaCl and KC1-KI1. *J. Phys. Chem.* **1955**, *59* (2), 118−127.
(48) Fei, L.; Lei, S.; Zhang, W.-B.; Lu, W.; Lin, Z.; Lam, C. H.; Chai, Y.; Wang, Y. Direct TEM Observations of Growth Mechanisms of Two-Dimensional MoS_2 Flakes. *Nat. Commun.* **2016**, *7*, 12206−12212.
(49) Kong, D.; Wang, H.; Cha, J. J.; Pasta, M.; Koski, K. J.; Yao, J.; Cui, Y. Synthesis of MoS_2 and $MoSe_2$ Films with Vertically Aligned Layers. *Nano Lett.* **2013**, *13* (3), 1341−1347.
(50) Choudhary, N.; Chung, H.-S.; Kim, J. H.; Noh, C.; Islam, M. A.; Oh, K. H.; Coffey, K.; Jung, Y.; Jung, Y. Strain-Driven and Layer-Number-Dependent Crossover of Growth Mode in van der Waals Heterostructures: 2D/2D Layer-By-Layer Horizontal Epitaxy to 2D/3D Vertical Reorientation. *Adv. Mater. Interfaces* **2018**, *5* (14), 1800382−1800391.
(51) Guo, J.; Li, F.; Sun, Y.; Zhang, X.; Tang, L. Oxygen-Incorporated MoS_2 Ultrathin Nanosheets Grown on Graphene for Efficient Electrochemical Hydrogen Evolution. *J. Power Sources* **2015**, *291*, 195−200.
(52) Chiappe, D.; Asselberghs, I.; Sutar, S.; Iacovo, S.; Afanas'ev, V.; Stesmans, A.; Balaji, Y.; Peters, L.; Heyne, M.; Mannarino, M.; Vandervorst, W.; Sayan, S.; Huyghebaert, C.; Caymax, M.; Heyns, M.; De Gendt, S.; Radu, I.; Thean, A. Controlled Sulfurization Process for the Synthesis of Large Area MoS_2 Films and MoS_2/WS_2 Heterostructures. *Adv. Mater. Interfaces* **2016**, *3* (4), 1500635−1500644.
(53) Ganta, D.; Sinha, S.; Haasch, R. T. 2-D Material Molybdenum Disulfide Analyzed by XPS. *Surf. Sci. Spectra* **2014**, *21* (1), 19−27.
(54) Kumar, P.; Viswanath, B. Horizontally and Vertically Aligned Growth of Strained MoS_2 Layers with Dissimilar Wetting and Catalytic Behaviors. *CrystEngComm* **2017**, *19* (34), 5068−5078.
(55) Kalita, H.; Krishnaprasad, A.; Choudhary, N.; Das, S.; Dev, D.; Ding, Y.; Tetard, L.; Chung, H.-S.; Jung, Y.; Roy, T. Artificial Neuron Using Vertical MoS_2/Graphene Threshold Switching Memristors. *Sci. Rep.* **2019**, *9* (1), 53−60.
(56) Zeng, L.-H.; Lin, S.-H.; Li, Z.-J.; Zhang, Z.-X.; Zhang, T.-F.; Xie, C.; Mak, C.-H.; Chai, Y.; Lau, S. P.; Luo, L.-B.; Tsang, Y. H. Fast, Self-Driven, Air-Stable, and Broadband Photodetector Based on Vertically Aligned $PtSe_2$/GaAs Heterojunction. *Adv. Funct. Mater.* **2018**, *28* (16), 1705970−1705980.
(57) Fu, L.; Hu, D.; Mendes, R. G.; Rummeli, M. H.; Dai, Q.; Wu, B.; Fu, L.; Liu, Y. Highly Organized Epitaxy of Dirac Semimetallic $PtTe_2$ Crystals with Extrahigh Conductivity and Visible Surface Plasmons at Edges. *ACS Nano* **2018**, *12* (9), 9405−9411.
(58) Politano, A.; Chiarello, G.; Kuo, C.-N.; Lue, C. S.; Edla, R.; Torelli, P.; Pellegrini, V.; Boukhvalov, D. W. Tailoring the Surface Chemical Reactivity of Transition-Metal Dichalcogenide $PtTe_2$ Crystals. *Adv. Funct. Mater.* **2018**, *28* (15), 1706504−1706511.
(59) Li, H.; Ko, T. J.; Lee, M.; Chung, H. S.; Han, S. S.; Oh, K. H.; Sadmani, A.; Kang, H.; Jung, Y. Experimental Realization of Few Layer Two-Dimensional MoS_2 Membranes of Near Atomic Thickness for High Efficiency Water Desalination. *Nano Lett.* **2019**, *19* (8), 5194−5204.
(60) Ma, H.; Chen, P.; Li, B.; Li, J.; Ai, R.; Zhang, Z.; Sun, G.; Yao, K.; Lin, Z.; Zhao, B.; Wu, R.; Tang, X.; Duan, X.; Duan, X. Thickness-Tunable Synthesis of Ultrathin Type-II Dirac Semimetal $PtTe_2$ Single Crystals and Their Thickness-Dependent Electronic Properties. *Nano Lett.* **2018**, *18* (6), 3523−3529.
(61) Wang, M.; Ko, T.-J.; Shawkat, M. S.; Han, S. S.; Okogbue, E.; Chung, H.-S.; Bae, T.-S.; Sattar, S.; Gil, J.; Noh, C.; Oh, K. H.; Jung, Y.; Larsson, J. A.; Jung, Y. Wafer-Scale Growth of 2D $PtTe_2$ with Layer Orientation Tunable High Electrical Conductivity and Superior Hydrophobicity. *ACS Appl. Mater. Interfaces* **2020**, *12* (9), 10839−10851.
(62) Tan, L.; Zeng, M.; Wu, Q.; Chen, L.; Wang, J.; Zhang, T.; Eckert, J.; Rummeli, M. H.; Fu, L. Direct Growth of Ultrafast Transparent Single-Layer Graphene Defoggers. *Small* **2015**, *11* (15), 1840−1846.
(63) Jung, D.; Kim, D.; Lee, K. H.; Overzet, L. J.; Lee, G. S. Transparent Film Heaters using Multi-Walled Carbon Nanotube Sheets. *Sens. Actuators, A* **2013**, *199*, 176−180.
(64) Celle, C.; Mayousse, C.; Moreau, E.; Basti, H.; Carella, A.; Simonato, J.-P. Highly Flexible Transparent Film Heaters Based on Random Networks of Silver Nanowires. *Nano Res.* **2012**, *5* (6), 427−433.

https://dx.doi.org/10.1021/acs.nanolett.0c01089
Nano Lett. 2020, 20, 3925−3934